Fusing and Short Circuit Interruption Behaviour of Metal Film Fuses

M. Lindmayer M. Luther

Institut für Elektrische Energieanlagen
Technische Universität Braunschweig
P.O. Box 3329, W-3300 Braunschweig
Germany

Summary

This paper presents some experimental results of current limiting and short circuit interruption behaviour of metal film fuses on alumina in comparison with a conventional fuse for semiconductor protection. Breaking tests were carried out in a 250 V–circuit with di/dt–values of 12 A/μs and 36 A/μs.

The fuse model shows very good interruption properties and in comparison with the conventional fuse the rated current is higher by a factor of nearly three at the same i^2t.

Additionally, numerical simulations of the melting characteristics are made. They show that the heat resistance between the alumina substrate and its cooled reverse side has to be taken into account.

1 Introduction

A metal film fuse is a new application of thick film technology to fuses. In comparison with conventional sand filled fuses, metal film fuses show some advantages with respect to the gap between the rated current and the short circuit let–through current. The heat dissipated from the constrictions and thus the rated current for a certain cross–section can be substantially increased by applying a metal layer on a thermally well–conducting substrate, such as Al_2O_3 and additionally cooling the bottom of the substrate. Thus a quick–acting device can be realized, which can be used for fast power semiconductor protection.

Under steady state conditions some experimental investigations with fast–acting miniature fuses were made by [1], where the fuselinks were manufactured by evaporating silver onto clear quartz disks. In [2] the time/current characteristics of different fuse designs were determined. In this case the conductor was formed by a burnt–in conducting paste on an alumina substrate as it is known from thick film technology of hybrid circuits [3]. The influence of the insulating substrate on the melting performance was investigated in [4] using a numerical simulation method. It was shown that silver thin film fuses on alumina are very sensitive to overloads.

Looking at the short circuit range it is known from conventional fuses that under adiabatic conditions the fusing performance depends only on the material and the minimum cross–section of the fuse conductor [5]. As in all types of fuses, the main factor influencing the voltage drop is the number of constrictions in series that is necessary for a safe interruption of short circuit currents [6]. Additionally, it is necessary to apply an arc extinction medium to assure satisfactory current breaking behaviour. Quartz sand has proved to show optimum behaviour in many respects. It is understood that the large surface area of the sand, together with the microscopic channels between the grains that allow the plasma to flow outward from the hottest zones, are responsible for this performance [5]. The difference with a fuse conductor on a ceramic substrate compared to conventional fuses is that the fuse conductor is only surrounded at one side by the sand.

The following studies were made to establish whether the experiences with conventional fuses can be transferred to metal film fuses in the short circuit range, because there is little information yet about their performance under these conditions.

2 Principal Structure of Metal Film Fuses

The principal structure of the investigated fuse models is illustrated in fig. 1. First the conductor is formed by a screen–printed and fired silver paste (4) on an Al_2O_3 substrate (5). The thickness of the substrate is 0.635 mm throughout, and its area is 1 × 2 inches. The typical thickness of the burnt–in layer is 8 μm, its specific electrical conductivity is $\kappa_p = 3.0 \cdot 10^4\ 1/(\Omega\text{mm})$. For carrying higher currents, the thickness of the layer is increased by electroplating up to 70 μm. The specific electrical conductivity of the electroplated silver layer (3) is typically $\kappa_{Ag} = 5.4 \ldots 5.8 \cdot 10^4\ 1/(\Omega\text{mm})$.

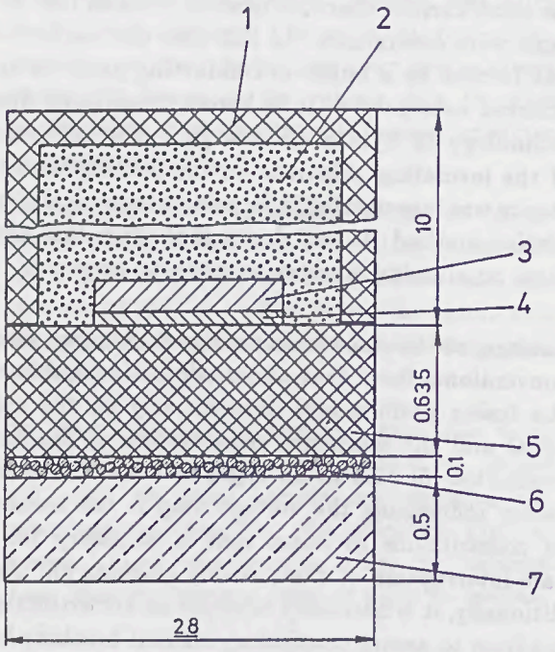

1 plastic case
2 sand filler
3 silver layer (20 ... 60 μm)
4 silver paste (8 μm)
5 Al_2O_3 substrate
6 heat–conducting adhesive
7 copper plate for cooling

Fig. 1: Principal structure of a metal film fuse (all dimensions in mm)

In order to provide a heat sink and to improve the mechanical strength, the substrate is connected to a copper plate (7) by a heat–conducting adhesive (6). The sand filler (2), which is necessary for optimum arc extinction, is contained in a plastic case (1) mounted on the substrate/conductor combination.

To study the influence of the number of constrictions, the experiments were carried out with two different fuse designs, shown in fig. 2. They consist of 5 or 7 notches in series and two parallel current paths. The width and length of each constriction is 0.5 mm. The geometries were chosen in an iterative process, taking into account the results of nominal current, voltage drop and a large number of interruption tests.

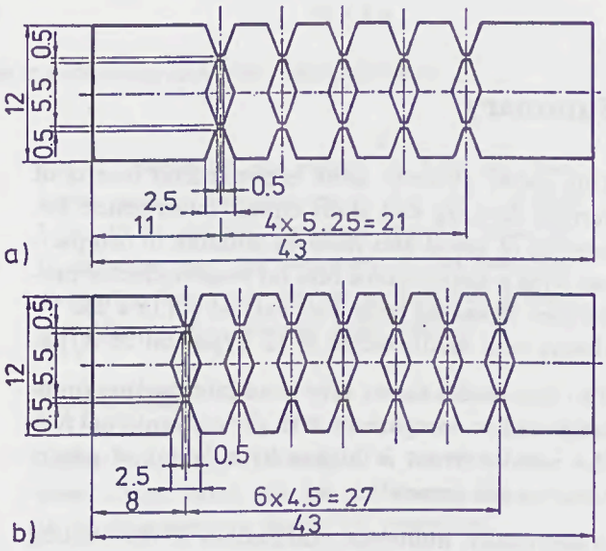

Fig. 2: Investigated fuse designs (all dimensions in mm)
a) 5 constrictions in series (type 5)
b) 7 constrictions in series (type 7)

3 Test Circuit and Experimental Arrangement

For first experiments under permanent current load in a low voltage DC circuit, the sand was omitted to allow temperature measurements in the metal film constrictions with an infrared thermometer [7]. Under these conditions the role of the quartz sand is negligible because of the main heat dissipation through the substrate.

By water–cooling the bottom of the fuses of fig. 1, the DC current was determined that the fuses are able to withstand for a long time ($t \to \infty$). It was found that 200 °C are not exceeded in the constrictions then. Though there is no precise coincidence with the definition in fuse standards, this current is referred to as *rated current* of the fuses.

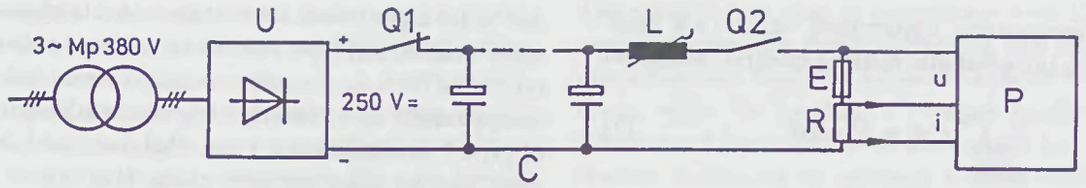

C	electrolytic capacitor bank (11 mF)	R	shunt (1 mΩ)
E	fuse element under test	Q1	safety switch
L	load inductance (21 and 70 μH)	Q2	make switch
P	transient recorder	U	rectifier

Fig. 3: Test circuit for breaking tests

The short circuit interruption experiments were carried out in the synthetic test circuit of fig. 3. The energy is supplied by a capacitor bank C charged to 250 V. Together with the load inductance L, it constitutes a resonant circuit of 330 Hz and 580 Hz respectively, for the chosen load conditions. The di/dt–values after closure of Q1 were set by L to 12 and 36 A/μs respectively, equivalent to peak short circuit currents of 38 and 115 kA under 50 Hz conditions. Provided the total interruption time is short in comparison with the resonant frequency, after interruption nearly the full capacitor charge voltage appears and remains across the fuse terminals. Under these conditions the tests are an approximation of a 250 V DC circuit and of the first critical stress in an AC circuit with 250 V momentary line voltage after clearing, respectively. In any case the circuit allows to study the fusing and interruption behaviour and to compare the influence of different fuse parameters. The current and voltage of the fuse are measured by a 20 MHz transient recorder (Nicolet Explorer 2019).

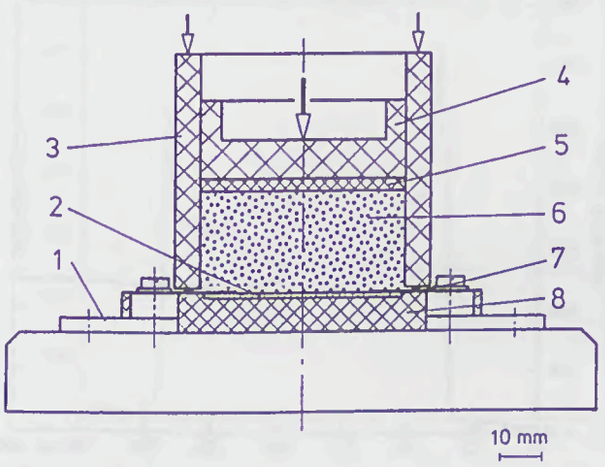

1	contact terminal	5	sealing strip
2	substrate with fuse conductor	6	sand filler
3	plastic case	7	seal
4	bakelized paper top	8	bottom plate

Fig. 4: Chamber for breaking tests

For the interruption tests the fuse model was modified to a demountable test chamber, illustrated in fig. 4. The fuse conductor (2) is contacted with soldered copper strips. The quartz sand (6) is filled into the case (3) and fixed by a top plate (4) under a constant force of 140 N. The inner volume of the chamber is 18 cm^3 and leads to a sand thickness above the conductor of about 12 mm.

4 Experimental Results

The object of the breaking tests was to get some knowledge about the influence of the conductor thickness and the number of constrictions on the fusing performance as well as the interruption capability. The fusing integral, depending on the total thickness of the conductor for the two fuse types at 12 and 36 A/μs, are shown in fig. 5 where every data point represents one interruption test.

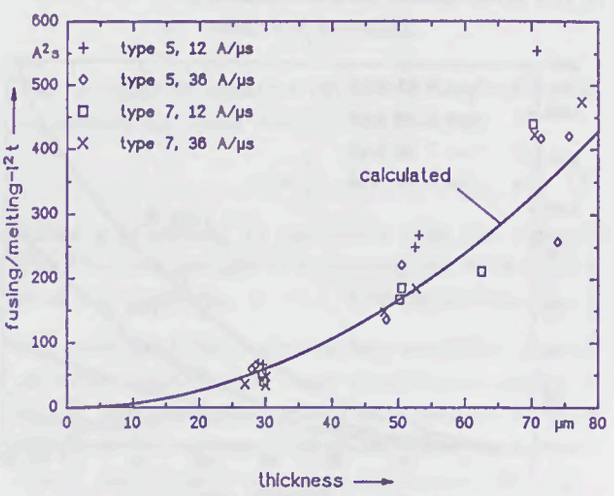

Fig. 5: Fusing and calculated melting integral for different thickness of the fuse conductors

The experimentally determined values are compared with the adiabatic melting integral calculated from [5]

$$\int_0^{t_m} i^2 dt = q^2 \cdot \Delta K \qquad (1)$$

where

i :	current
t_m :	time when melting point is reached
q :	minimum cross–section
ΔK:	material constant ("melting impulse"[5]) ($6.7 \cdot 10^4$ A^2s/mm^4 for Ag)

As a simplification, the conducting sandwich consisting of 8 μm conducting paste plus electroplated silver is treated as a uniform metal with the ΔK value of solid silver.

It can be seen from fig. 5 that especially for larger thicknesses the calculated melting integral is less than the fusing integral. Taking into consideration that the paste has a resistivity of about double the value of Ag and the electroplated silver of about 10 to 15 % higher than solid silver would yield fusing integrals of roughly 25 to 15 % lower, depending on the total thickness of the sandwich. According to [5] the $\int i^2 dt$ necessary to establish the arc is nearly identical with the value to heat the notches up to the melting point. The results from fig. 5 show that some additional energy, though definitely smaller than the value for complete melting and boiling, is necessary.

In fig. 6 the breaking integrals for the same experiments are summarized. There is no dependence on di/dt in the investigated range. Both types with 5 and 7 constrictions interrupt the current properly in the investigated range, where type 7 acts faster due to its higher total arc voltage. At a thickness of more than 50 μm type 5 shows an increase of breaking times (= time until the residual current tail has disappeared) up to 28 ms, while the breaking times of type 7 are still below 1 ms. Failures could, however, not be observed with these fuse types. On the other hand breaking tests with fuses of only 4 notches in series have shown that they are not able to break the current under these conditions.

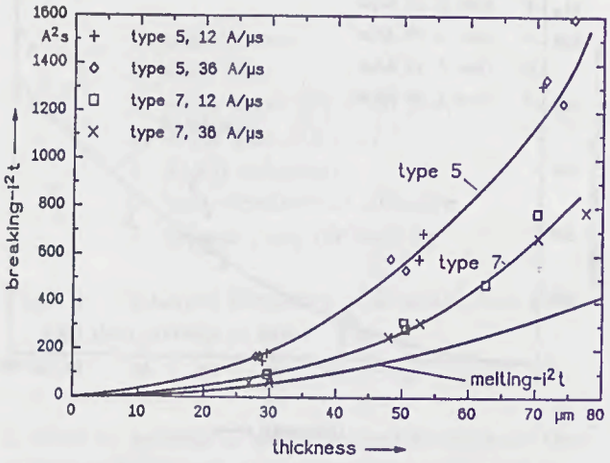

Fig. 6: Breaking integral for different thickness of the fuse conductors

A typical oszillogram of a breaking test of a metal film fuse (type 7) is shown in fig. 7. The determined rated current for this fuse pattern is 100 A when the bottom is cooled. For a current rise of 36 A/μs the let–through current is 2.7 kA and the breaking time is 320 μs. The fusing integral of this metal film pattern is 185 A^2s, the breaking integral is 313 A^2s, respectively.

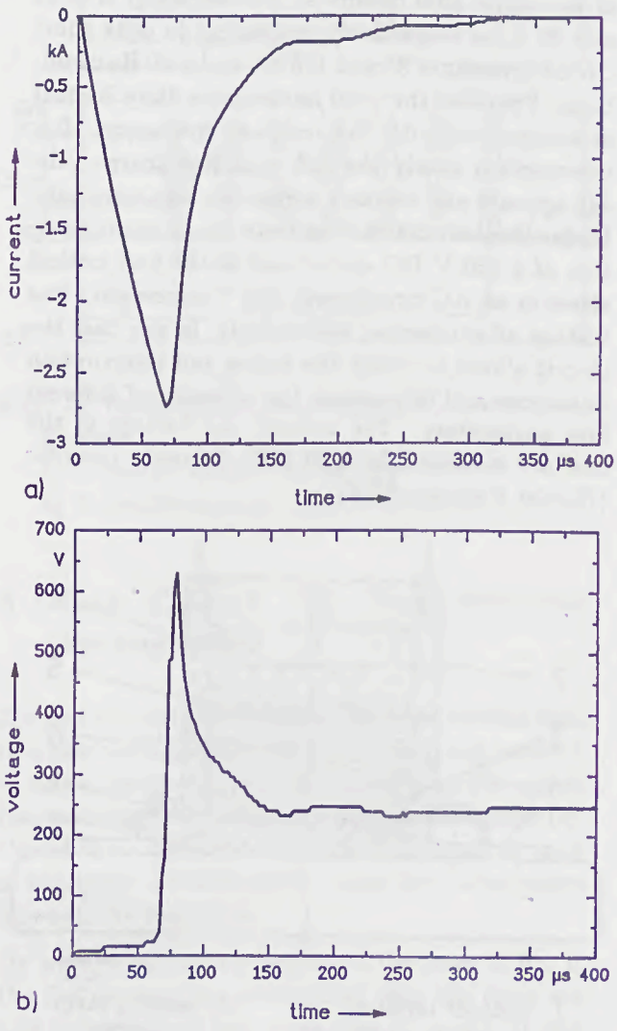

Fig. 7: Breaking test of a metal film fuse (type 7, d = 45 μm, di/dt = 36 A/μs)
a) current distribution
b) voltage distribution

To compare the short circuit behaviour of metal film fuses, breaking tests were carried out with conventional semiconductor fuses. Fig. 8 shows results in the same time range and under the same conditions as in fig. 7 for a conventional semiconductor fuse (35 A/500 V) of approximately the same breaking $\int i^2 dt$. It consists of a silver strip 70 μm thick with a pattern of two parallel paths of 7 constrictions in series. The let–through current is somewhat less than for the metal film fuse (2.3 kA), but current zero is only reached after 3.5 ms. The fusing and breaking integrals are 102 A^2s and 274 A^2s. Comparing the arc voltage of the different fuses, it can be seen that the metal film fuse has a higher peak voltage, resulting in a faster current decay.

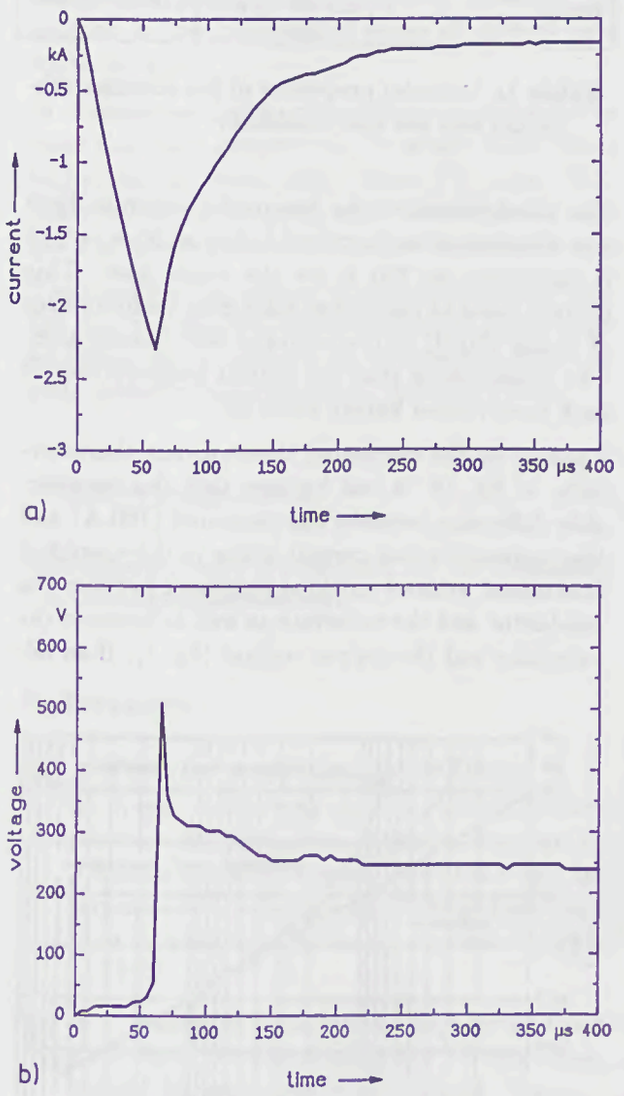

Fig. 8: Breaking test of a conventional semiconductor fuse (I_r = 35 A, di/dt = 36 A/μs)
a) current distribution
b) voltage distribution

The results show that in comparison with the conventional fuse the rated current of the described metal film fuse sample is higher by a factor of nearly three, while the breaking i^2t–values hardly differ. The time of the cessation of the current tail is even shorter, indicating in tendency a faster recovery of the gap.

5 Calculated melting characteristic

The melting characteristic of the metal film fuses was studied using the general purpose FEM program ANSYS [8]. The feature of this program is to solve the steady state and transient thermal–electrical coupled field problem with temperature dependent material properties.

The governing differential equation for the heat flow in a conducting solid is given by

$$div(\lambda \cdot gradT) - \rho \cdot c\frac{\partial T}{\partial t} = -\eta \qquad (2)$$

while the Laplace equation of the electrical current flow is described by

$$div\vec{J} = div(\kappa \cdot grad\varphi) = 0 \qquad (3)$$

where

λ: thermal conductivity
T: temperature
t: time
ρ: density
c: specific heat
η: power density
κ: electrical conductivity
$\vec{J}$: current density vector
φ: electrical potential

The coupling of equation (2) and (3) is given by the expression for *Joule heating* described as

$$\eta = \frac{1}{\kappa} \cdot J^2 \qquad (4)$$

where η is defined as generated heat per volume. The iterative solution procedure of the ANSYS program for equations (2) and (3) is treated in [9].

The generated finite element fuse model for the calculations under steady state conditions is shown in fig. 9. Because of symmetry it represents only an eighth section of type 7 (fig. 2b). The model consists of the ceramic substrate (thickness 0.635 mm) and the applied fuse conductor with a thickness of 50 μm. The current load (DC only) is applied at the nodes of the constriction on the left side, while the

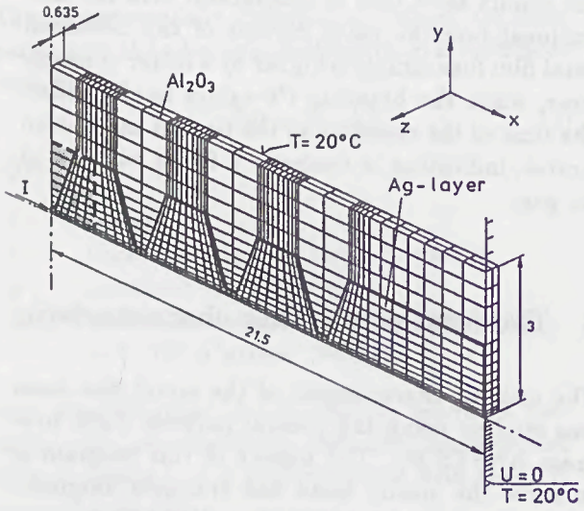

Fig. 9: Steady state FEM fuse model (all dimensions in mm)

electrical potential on the right side of the conductor is fixed to zero. The cooled reverse side of the substrate, as well as the right side of the fuse (fuse terminal), is kept at a temperature of 20 °C. The heat dissipation by convection and radiation can be neglected because thermal conductivity plays the major role in this case. It was assumed first that there is no additional heat resistivity between the conductor and the substrate and between the substrate and the copper plate (fig. 1) of the real fuse.

The melting performance in the overcurrent and short circuit range was computed by increasing the applied current and calculating the time to reach the silver melting point (960 °C). As the calculations proved that the heat conduction between adjacent constricted sections is negligible, the FEM model of fig. 9 was modified into a one constriction fuse model with a finely subdivided ceramic substrate in z–direction. The geometry is indicated by a dashed line in fig. 9.

The temperature dependent material properties (electrical resistivity ϱ, thermal coductivity λ, specific heat c) of the Al_2O_3 substrate and the conductor are linearisized by

$$X(T) = X_0[1 + \alpha_{\varrho,\lambda,c}(T - T_0)] \qquad (5)$$

where

X: ϱ, λ, c
α_X: temperature coefficients of ϱ, λ, c
T: temperature

and the index 0 is used for the properties at 20 °C.

The properties and coefficients for the materials taken from the literature [10, 11, 12, 13] are shown in table 1. The electrical resistivity of the fuse conductor results from the parallel layers of the paste and the plated silver shown in fig. 1. It is higher than the pure silver value ($\varrho_{Ag} \approx 1.5 \cdot 10^{-5}$ Ωmm).

property		conductor	Al_2O_3 substrate
electrical resistivity	ϱ_0	$1.995 \cdot 10^{-5}$ Ωmm	–
	α_ϱ	$4.08 \cdot 10^{-3}$ 1/K	–
thermal conductivity	λ_0	0.428 W/mmK	$24 \cdot 10^{-3}$ W/mmK
	α_λ	$-1.4 \cdot 10^{-4}$ 1/K	$-1.0 \cdot 10^{-3}$ 1/K
specific heat	c_0	0.233 J/gK	1.01 J/gK
	α_c	$4.29 \cdot 10^{-4}$ 1/K	$4.59 \cdot 10^{-4}$ 1/K
density	ρ	$10.5 \cdot 10^{-3}$ g/mm³	$3.75 \cdot 10^{-3}$ g/mm³

Table 1: Material properties of the alumina substrate and the fuse conductor

The rated current of the fuse model shown in fig. 9 was determined as described before as 55 A, which is equivalent to 220 A for the whole fuse. This current leads to calculated maximum temperatures of about 180 °C in the center of each constriction. The results show that the hottest temperatures of each constriction hardly differ [9].

Looking at the calculated time/current characteristics of fig. 10, it can be seen that the considerable difference between the measured (100 A) and the computed rated current is due to the simplified fuse model without any heat resistance between the conductor and the substrate as well as between the substrate and the copper coolant (fig. 1). If an ad-

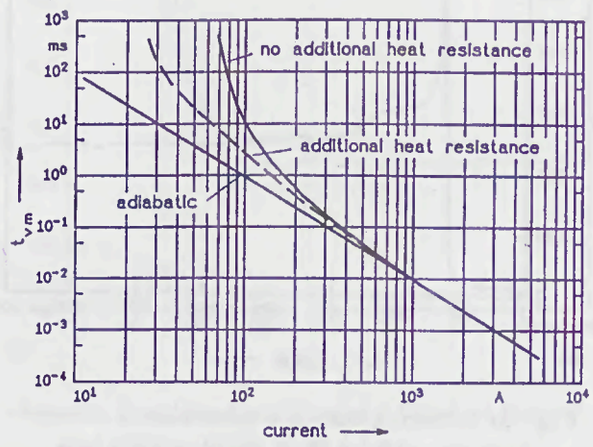

Fig. 10: Calculated time/current characteristics for one eighth section

ditional heat resistance is taken into consideration, the curve shifts to lower nominal current values. First estimations were carried out with the heat resistance of a 0.1 mm thick layer of heat–conducting adhesive (dashed line). The results are in much better agreement. It can be concluded that this resistance plays the major role in this case, and that its reduction will further improve heat dissipation from the notches.

6 Conclusion

The investigated metal film fuses have a quick–acting fusing performance. They additionally showed an excellent short circuit breaking behaviour in the investigated range of current rises up to 36 A/μs.

In comparison with conventional semiconductor fuses the rated current can be nearly three times higher for the same short circuit i^2t–value. This effect is due to the good heat dissipation through the Al_2O_3 substrate cooled at the reverse side.

The results of the numerical calculations show that the heat resistance of the intermediate layers must be taken into consideration to simulate the complete melting characteristic of metal film fuses.

Acknowledgement

This research work is supported by the **Deutsche Forschungsgemeinschaft.**

References

[1] A. F. Howe, D. de Cogan, P. W. Webb, N. P. M. Nurse: *Measuring the Pre–Arcing Temperature of High–Breaking–Capacity Fuselinks by Thermal Imaging*, Proceedings of the 2nd International Conference on Electric Fuses and their Applications, Trondheim – Norway 1984, p. 12–23

[2] A. J. Marriage, B. McIntosh: *High Speed Thick Film Fuses*, Proceedings of the 5th European Hybrid Microelectronics Conference, Stresa – Italy 1985, p. 282–287

[3] H. Reichel (Publ.): *Hybridintegration*, Technologie und Entwurf von Dickschichtschaltungen, Hüthig–Verlag, Heidelberg 1986

[4] D. de Cogan, M. Henini: *TLM Modelling of Thin Film Fuses on Silica and Alumina*, Proceedings of 3rd Conference on Electrical Fuses and their Applications, Eindhoven, the Netherlands 1987, p. 12–17

[5] H. Johann: Elektrische Schmelzsicherungen für Niederspannung, Springer–Verlag, Berlin, Heidelberg, New York, 1984

[6] A. Wright, P. G. Newbery: *Electric Fuses*, IEE Power Egineering Series 2, Peter Peregrinus Ltd., London – New York 1982

[7] M. Hofmann: *Experimentelle und rechnerische Untersuchungen von Ansprechkennlinien und Alterungsvorgängen bei Sicherungsschmelzleitern*, Thesis TU Braunschweig 1984

[8] G. J. DeSalvo, R. W. Gorman: *ANSYS Users Manual Rev. 4.4*, Swanson Analysis Systems Inc., Houston PA, USA 1989

[9] M. Lindmayer, M. Luther: *Static and Dynamic FEM Calculation of Current and Temperature Distribution in Metal Film Fuses*, Proceedings of the 5th International ANSYS Conference, Pittsburgh PA – USA 1991

[10] F. Kohlrausch: *Praktische Physik*, Band 3: Tafeln, B. G. Teubner, Stuttgart 1968

[11] A. Tslaf: *Combined Properties of Conductors*, Elsevier Scientific Publ. Company, Amsterdam, Oxford, New York, 1981

[12] R. C. Buchanan: *Ceramic Materials for Electronics*, Marcel Dekker Inc., New York, Basel, 1986

[13] Y. S. Touloukian: *Thermophysical Properties of Matter, Vol. 5: Specific Heat*, Plenum Press, New York 1975

Session 5A

MOTOR CONTROL FUSES